Journal of Engineering Science and Technology
Vol. 16, No. 4 (2021) 3435 – 3454

USING AGRICULTURAL WASTE AS BIOSORBENT FOR HAZARDOUS BRILLIANT GREEN DYE REMOVAL FROM AQUEOUS SOLUTIONS

SAGA M. BADR, ISRA'A S. SAMAKA*

Department of Environmental Engineering, College of Engineering, University of Babylon, Hilla, 51001, Babylon, Iraq
*Corresponding Author: israasamaka@yahoo.com

Abstract

This study is concerned in the potential use of agricultural wastes (watermelon peels, WP) for removal of Brilliant Green dye (BGD) from coloured effluents as they keep growing nowadays because they are industrial wastes and are low-cost as they exist in abundance and this process is considered as wastes management. Different techniques are used for characterization study before and after BGD removal. These techniques are surface area (SBET), FTIR, SEM, and SPM. Effects of different parameters on BGD removal were studied, consisting of pH of dye solution, contact time, biosorbent dose, initial concentration of dye. The isotherm analysis revealed that the equilibrium data were greatest simulated with the model of Langmuir and the maximum uptake of BGD was 25 mg/g. The results indicated that WP can be utilized as non-hazardous agro-waste for the removal of BGD from aqueous solutions.

Keywords: Agricultural waste, Biosorption, Cationic dye, Isotherms.

1. Introduction

Dyes and pigments released to the natural environment are increased as a result of the development of technologies and industrial activities. Worldwide, over 7 x 10^5 tons of dyes and pigments are produced annually [1], and approximately 90% of this ends up on fabrics [2]. Dyes usually are commercially synthesized with complicated aromatic molecular structures, and they have extensive applications in textile, leather, plastic, rubber, paper industries, and construction industries [3-6]. Due to the development of these industries, large quantities of coloured water are produced [7; 8]. The industry of textile alone accounts for two-thirds of the total dye production and about 10 to 15% of the used dyes come out through the effluent which is caused serious dangers to the public health and the environment [9; 10]. So, water contamination is considered the principal cause of environmental contamination at the present time. Because of these coloured effluents, sunlight cannot be reached to aquatic plants which are essential for various biotic events like photosynthesis [7, 11].

Various physiochemical techniques including coagulation [12], electrochemical technique [13, 14], nanofiltration membranes [15, 16], photocatalytic degradation [17, 18], membrane separation [19], ultrasonic technique [20, 21], ozonation [22], advanced oxidation [23], and microfiltration [24, 25], photo-degradation [26, 27], aerobic degradation [28, 29], and adsorption [30, 31] have been found significantly effective in dealing with these wastewaters. However, these methods have limitations like coagulation leads to a huge amount of waste products with high disposal costs [32-34]. Conventional biological methods are expensive so they cannot be used to treat a wide range of coloured wastewater. The ion-exchange technique is expensive and cannot be used with such a wide range of dyes [35]. Adsorption is considered to be a simple and effective technique, and an ideal cheaper alternative can be used, which gets the whole removal of contaminants [36, 37].

The best extensively adsorbent used for the colour removal from different discharges is activated carbon because it possesses a high surface area with micropore and mesopore structures and is known as efficient adsorbents for gas and liquid [38]. The chief concerns related to using activated carbon are regeneration and trouble of filtration from effluent after use it [38]. Using biomass keeps growing nowadays because they are industrial wastes, including agricultural wastes and they exist in abundance and low-cost. So, many investigators have attentive to the development of low cost, nonconventional agricultural wastes as an alternative adsorbent of activated carbon, such as Peanut shell, Rice husk ash, and fruit peels, such as orange peels, pomegranate peel, and Banana peels and Jackfruit peels [8, 15]. Therefore, the biomass used adsorption process is considered as green technology when it does not change the properties and react to other chemicals as mixed with chemicals containing wastewater.

Fruit and vegetable peel contains 51-58% oxygen, which confirms the existence of fiber and carbohydrate. Higher amounts of cellulose, hemicellulose, and polymers are potential bio-adsorbents for wastewater decolourization because they are rich with functional groups (such as hydroxyl, carboxyl, and amine), which can easily attract cationic pollutants and make them [39]. The nature of fruit and vegetable peel surface can be evaluated by calculating the net amount of basic and acidic sites on it during the investigation of surface charges of different fruit and vegetable peels, and it is observed that all peels studied including watermelon peels are more suitable for the removal of cationic contaminants from aqueous solution [39].

The need for developing efficient methods for dyes and other pollutants from waters and wastewaters is not only because of the effects of the effluents of the textile industry, but also because of the shortage of freshwater that resulted from climate changes [40-42], the increase in urbanisation [43-45], effluents of other industries such as concrete [46-49], cement industries [50-53], and also because of domestic wastes and wastewaters [54-56].

This work is aimed to evaluate the natural watermelon peels, WP as biosorbent for removal of BGD from its aqueous media in batch mode. The biosorbent preparation with surface characterization was critically talked over. Various factors were investigated to discover the optimum conditions for dye biosorption. The equilibrium data were fitted using the Langmuir and Freundlich isotherm model. The attained results will supplement the other works of utilizing fruits peels for removal of this category of contaminants.

2. Material and Procedures

2.1. Preparation of biomass sorbent

The biomass sorbent of watermelon peels (WP) was chosen because of its locally available and eventually discarding nature as the agro-waste material. So, this fruit was gotten from a local Iraqi market, and peels of watermelon were washed a number of times using tap water, after that distilled water. For easily drying, WP was cut into small parts. Afterwards, the peels were dried through sunlight for seven days to eliminate all the humidity content. Then, the hot water (70 ºC) was used to wash the peels to eliminate water-soluble substances, dust, etc. and dried by an oven at 85 ºC for 48h. Finally, the biosorbent was ground and sieved through 100 mesh [57]. The prepared biosorbent was saved in airtight bottles to use it for the next experiments.

2.2. Characterization techniques of WP

The surface area, S_{BET} of biosorbent was performed using the isotherms of nitrogen adsorption-desorption attained by an analyser of BET surface area, Model No. Qsurf 9600, Themo Finnegan Co., the USA in relative pressure < 0.35 p/pº. The investigations on the changes resulted after and before brilliant green dye (BGD) onto WP were performed using different tests. FTIR spectroscopy (SHIMADZU, IRPrestige-21, Japan) was dependent on discovering the functional groups that existed on the surface of biosorbent studied in the series of 4000-400 cm^{-1} using KBr tablet way. The investigations on the changes of the surface and shape of natural WP before and after BGD removal were achieved by using images with high accuracy gotten by scanning electron microscopy (SEM; TESCAN, Mira3, France). The topography of natural WP was investigated by the SPM test (SPM AA300, Advanced Angstrom Inc., USA with contact style of AFM).

2.3. Chemicals

Reagents with analytical rank were used in this work. A cationic BGD used in this work was bought from Sigma Chemical Co. (USA). It is described as ammonium, 4 (diethylamino) - alpha - (phenylbenzylidene). It is categorized as a cationic dye basic green 1 with C.I. of 42040; MW= 482.63 g/mol; 624 nm λ_{max}; molecular formula= $C_{27}H_{34}N_2O_4S$ the structural formula of BGD is presented in Fig. 1. Dissolving an appropriate amount of dye powder using double-distilled water for preparing a solution with a strength of 10^3 mg/l. The dilution method was used to

get the other strengths of BGD solutions from the stock solution. The adjustment of pH values was performed using 0.1M HCl or NaOH as required.

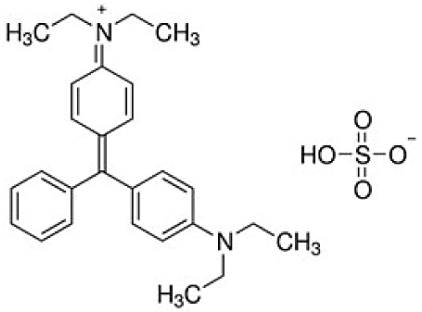

Fig. 1. The structural formula of BGD [7].

2.4. Biosorption investigates

A batch system was dependent on performing all the experiments of BGD biosorption utilizing WP at ambient temperature (30±2 ºC), using numbers of 250 ml conical flasks containing 100 ml solution of BGD. The influences of operating factors on the biosorption rate were observed to define the best conditions for biosorption process and get the greater number of equilibrium data that are suited for the determination of interactive material activity and isotherm of biosorption. These factors included the study of the pH of dye solution, contact time, biosorbent mass, and initial dye concentration. Table 1 shows the major varied parameters used in these experiments.

Table 1. Major varied experimental parameters in batch experiments.

Parameter	Range	Purpose
pH	2, 4, 5, 6, 7, 8, and 9	To find the optimum pH of removal
Contact time, min.	10 - 120	To discover the equilibrium time
Dose of biosorbent, g / 100 ml	0.05, 0.1, 0.2, 0.3, 0.4, 0.5, 0.6, 0.7, 0.8, 0.9, 1, 1.1, 1.2, 1.3, and 1.4	To find the optimum biosorbent dose
Initial dye concentration, mg/l	10, 20, 30, 40, 50, 60, 70, 80, 90, and 100	To show the effect of dye concentration on bisorption process and to plot the equilibrium isotherm curves

After completing each experiment, a sample of the solution was taken from every flask and the sample was filtered and analysed for finding the amount of remaining dye concentration using a UV-VIS spectrophotometer with a double beam (UV/VIS-6800 JENWAY) at 624 nm as maximum wavelength.

The dye uptake, q_e (mg g^{-1}) and biosorption efficiency ($R\%$) at equilibrium time were calculated using Eq. (1) and Eq. (2), respectively [23]:

$$q_e = \frac{C_\circ - C_e}{M} V \quad (1)$$

$$R\% = \frac{C_\circ - C_e}{C_\circ} * 100 \quad (2)$$

As, C_o and C_e are primary and equilibrium concentrations of BGD (mg/l), M is the quantity of biosorbent (g), then, V is the volume of BGD solution (l). Investigation on the pH value when the final and initial pHs are the same and the charge of biosorbent surface is neutral at this pH value (point zero charges, pH_{pzc}) is a fundamental characteristic that helps to comprehend which ionic types can be sorbed by biosorbent at desired pH. The pH_{pzc} of WP is fined based on the previous conventional method [58], using batch equilibrium mode. The amount of 0.5 g of WP was put in conical flasks which are contained 50 ml of 0.1M NaCl solution. The initial values of pH (pH_i) (2-9) were organized using 0.1 M solution of NaOH or HCl. After that, the suspensions obtained were agitated at 150 rpm for 24 hr. After that, WP was filtered, and the ending pH value of the solution was tested. The pH_{pzc} is obtained from the point of interception zero with the curve obtained by plotting the ΔpH vs. pH_i.

3. Results and Discussion

3.1. Characterization of WP

Detailed values of physicochemical characteristics of natural biosorbent were recorded in Table 2. The S_{BET} of biosorbent was calculated following the method of Brunauer-Emmett-Teller (BET) founded by the linear part of the N_2 adsorption-desorption isotherm [59].

Table 2. Elemental composition (%w/w) and physicochemical characteristics of natural WP.

	Elemental composition (%w/w)						
	C	**O**	**N**	**H**	**S**	**Ash**	**L.O.I**
WP	42.70	31.07	0.92	6.11	1.41	7.65	10.14
Physicochemical characteristics							
Surface area, SBET (m^2 g^{-1})				18.75			
Moisture content %				12.6			
Particle density (g/ml)				1.07			
Bulk density (g/ml)				0.42			
Point zero charge (pH_{pzc})				5.0			

The FTIR spectra are an essential analysis to sense the useful groups that exist on the biosorbent surface to explain the bonding ways of BGD ions with these functional groups. So, FTIR was performed upon WP before and after BGD biosorption as shown by Figs. 2(a) and (b) to elucidation the locations of these active groups along with the changes in their locations after the biosorption process. Figure 2(a) displays the FTIR spectra of WP before BGD ions biosorption. Different IR bonds are looked at that indicated different functional groups regarding to their wavelengths (cm^{-1}).

The wide and deep band at 3387 cm^{-1} is due to the stretching vibrations of -OH revealed the lignin, pectin, or cellulose and N-H which is related to amine functional groups [39, 57]. The second peak was looked at the frequency at 2920.23 cm^{-1} which is referred to -CH asymmetric stretching vibrations of groups of methyl and methoxy, while 2852.72 cm^{-1} related to the symmetric stretching bond of -CH. The peak at 1741.72 cm^{-1} denotes to -C=O stretching of esters or carboxylic acid. The frequency at 1622.13 cm^{-1} is assigned to the asymmetric vibrations of the ionic carboxylic group ($-COO^-$), but the band at 1419.61 cm^{-1} revealed the symmetric vibrations of the same groups.

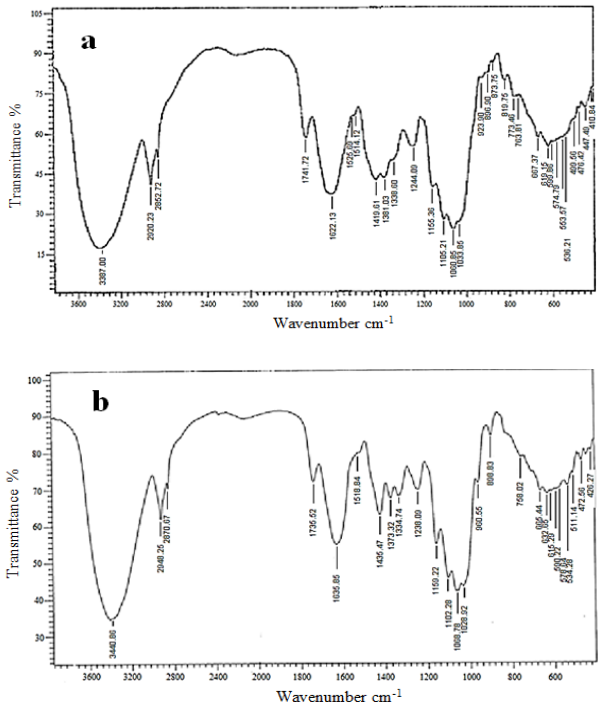

Fig. 2. FTIR analysis for (a) natural WP (b) BGD loaded WP.

The frequencies at 1525.69 cm^{-1} and 1514.12 cm^{-1} are assigned to the aromatic C=C group stretching vibration in aromatic rings [57]. The frequency at 1381.03 cm^{-1} and 1338.60 cm^{-1} are referred to $-COO^-$ symmetric stretching of pectin [57]. The peaks in the range of 1300-10^3 cm^{-1} referred to the stretching vibrations of C-O-C and C-O groups of carboxylic acids, esters, alcohols, and phenols [39]. The peaks at 923.90, 896.90, 873.75, and 819.75 cm^{-1} represent the vibration of symmetric stretching of N-H of primary and secondary amines. The frequencies at 773.46 cm^{-1} and 763.81 cm^{-1} referred to C-N stretching. All peaks fewer than 700 cm^{-1} referred to alkyl halides compounds with C-Br (stretching vibration) bond. Thus, the IR spectral shows that the surface of WP before BGD biosorption is rich in hydroxyl and carboxylic groups, which they act as proton donors to bind the cation BGD along with the other medium and weak functional groups participating in biosorption process.

These findings can be shown through Fig. 2(b). After WP is loaded with BGD, absorption peaks are shifted, new peaks are looked, and other are disappeared. These variations may be affected by association of revers ions with hydroxylate and carboxylate anions signifying that the dye biosorption is controlled by hydroxyl, carboxyl, and carbonyl groups. So, the biosorption of BGD onto WP can be due to (i) chemical reaction between functional groups and dye ions (ii) electrostatic interaction between dye ions and the electron contained in sites on surface of biosorbent, and (iii) hydrogen bonding interactions and weak physical forces, van der Waals between BGD ions and biosorbent. As the carboxyl group of each biosorbent interacts with the positively charged nitrogen moiety of the BGD molecule, also the hydroxyl group of biosorbent bonds with the ammonium ion, or aromatic ring in dye molecule via the hydrogen bonding. So, both physical and chemical adsorption are involved in dye removal [60, 61].

The shape and surface texture morphology were investigated by the SEM technique for WP before and after biosorption of BGD as shown by Figs. 3(a) and (b). There are significant features of an irregular, rough surface with substantial layers of rough heterogeneous pores, cavities, and ravines that are favourable properties as increase the biosorption of dye through the improvement of break easily binding of BGD ions onto the active sites. These observations are consistent with these were reported in the literature [60, 61].

After the BGD biosorption onto WP (Fig. 3(b)) and related to Fig. 3(a), a number of intense graphic changes were clear. The surface of WP appeared smooth and disappearing of a few pores which are seen earlier. These changes indicated both physical and chemical reaction between BGD ions and both surface and inner pores of biosorbent. Similar observations are noticed by Mohammed and Samaka [60].

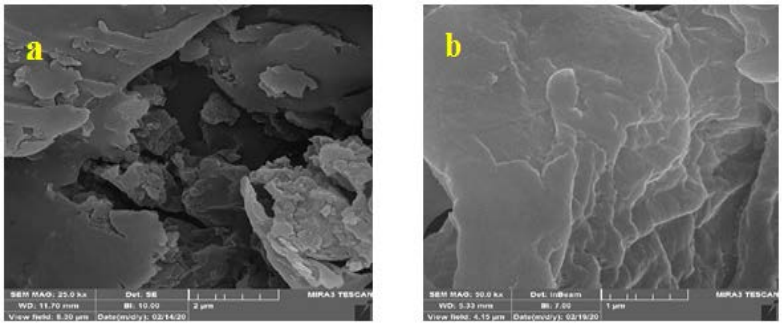

Fig. 3. The SEM micrograph pictures of natural WP (a) before BGD removal (b) after BGD removal.

The topography characteristics of biosorbent before and after removal of BGD at the same scale were investigated and Figs 4(a) and 4(b) explained the results. Before BGD removal, the 3D images show that each material has an amorphous and rough surface with heterogeneous, which enhance adhesion of the dye ions, but after BGD removal, surface roughness and surface area were reduced as 3D profiles show how the number and form of the dotes vary as the quantity of BGD ions deposited onto the surface of biosorbent and covered biosorbent surface leading to reduce the surface roughness and surface area. The essential data obtained by this analysis are listed in Table 3.

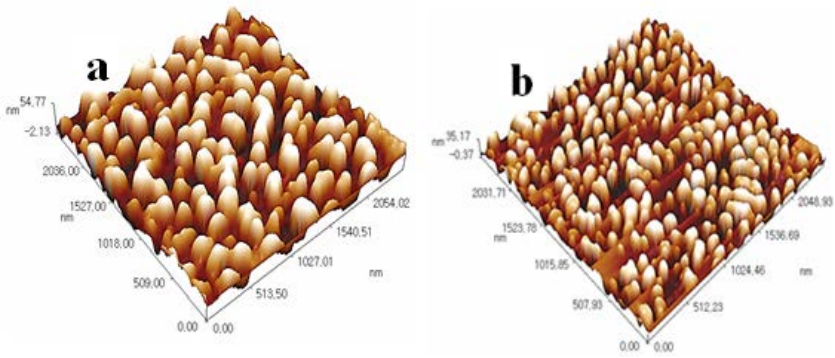

Fig. 4. Scanning probe microscope for WP: (a) before BGD biosorption (b) after BGD biosorption.

Table 3. WP characteristics before and after biosorption of BGD by SPM.

Character	WP	
	Before	After
***Sa* (roughness average) (nm)**	14.2	8.89
***Ssk* (surface skewness)**	0.00245	0.131
Ten-point height (nm)	56.8	35.4
***Sar* (surface area ratio)**	25.2	14.6
***Sk* (core roughness depth) (nm)**	49.5	30.9

3.2. Parameters influencing the BGD biosorption

3.2.1. The influence of dye solution pH

The dye solution acidity is the essential factor governing the adsorption technique in aqueous solution [32]. The functional groups found on the surface of adsorbent is affected by this parameter; also, it defines the solubility of the contaminant in the aqueous media. The competition among the contaminant ions that sorbed to the adsorbent active sites is also affected. Figure 5 displays the deviation of the removal efficiency of BGD with varying solution pH in terms of contact time using WP. The biosorption efficiency was enhanced with the increase of contact time for all pH ranges and became slow near the equilibrium. It was increased from 78.86 to 98.40% with the rise of solution pH from 2 to 9. So, it was evident that ions biosorption strongly depended on pH. At pH more than 8, there is no significant effect on BGD biosorption. The optimum removal of dye was reported at pH 8, and it was reported as 98.35%. Therefore, the next experiments were carried at pH 8. The lowest biosorption of dye onto WP was looked at pH 2 as the movement of more concentrations of H^+ ions present and the biosorbent surface is bounded by hydrogen ions which contest with dye cations for the biosorption places found in biosorbents, inhibiting the BGD ions from reaching these places. So, the increase of solution pH will increase the negative charge intensity on the surface of biosorbent and increase the affinity of the cationic dye's site toward biosorption. Similar notes were in agreement with some earlier studies [60, 61]. The point of zero charges (pH_{pzc}) is an important parameter for determining the type of surface-active centres and the adsorption ability of the surface.

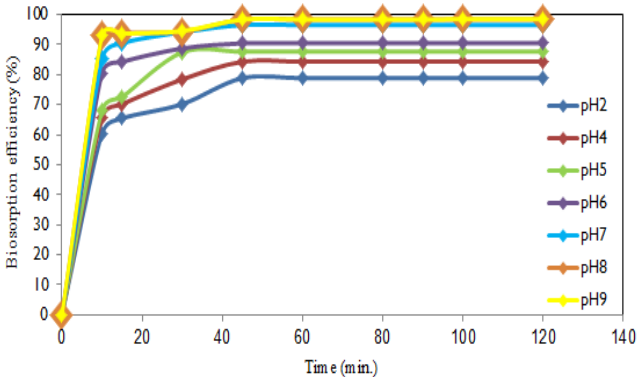

Fig. 5. Influence of initial pH in terms of contact time at various pHs on the biosorption efficiency of BGD at the strength of 50 mg/l, and 250 rpm for 120 min using WP with a dose of 0.8 g/100 ml.

The pH_{pzc} of the WP surface was reported as the point of intersection of pH_i vs. ΔpH presented that the pH_{pzc} of WP happened at pH 5 at which the surface of WP is neutral as illustrated in Fig. 6. As pH lower than 5, the WP surface is dominated by the positive charges, so repulsion between the cations of dye and each of biosorbent has happened and decreased the BGD removal. But, as the pH higher than 5 the biosorbent surface is dominated by negative charges due to the presence of OH^- groups and come to be more satisfactory for cations of dye removal due to the attraction of electrostatic forces.

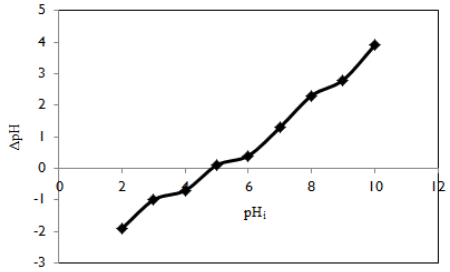

Fig. 6. Finding of point zero charges (pH_{pzc}) of natural WP.

3.2.2. The influence of contact time

The study of the finding the equilibrium time is needed to identify the possibility of binding for active sites occupied by BGD and completing the removal of it. Generally, the removal efficiency or uptake of dye increases to a certain extent with increasing of contact time. Further increase in contact time does not be significant in the removal of dye on the available active sites found onto the adsorbent. The mass of dye removed at equilibrium time refers to the adsorbent's maximum adsorption capacity under those operating factors. Figure 7 illustrates that the uptake of BGD is affected by contact time. The maximum uptake was reported as 6.2 mg g^{-1}. Sorbed amount of BGD increased with increasing contact time and remained relatively constant after equilibrium time. Through Fig. 7, it can be noticed that the biosorption process is divided into two stages, fast and slow stage. The first stage comprised a rapid initial removal efficiency of dye when it was over 90% within the first 10 min. In the second stage, a slow removal rate is followed by attainment equilibrium at 60 min. There was no important change in BGD removal rates after this time. This can be interpreted by the fact that at the beginning, a great number of surface sites exist for biosorption of BGD ions and there is higher contact between the dye and surface of biosorbent, but after equilibrium time, the remaining surface sites are limited and difficult to occupy these ions. These observations are consistent with other studies.

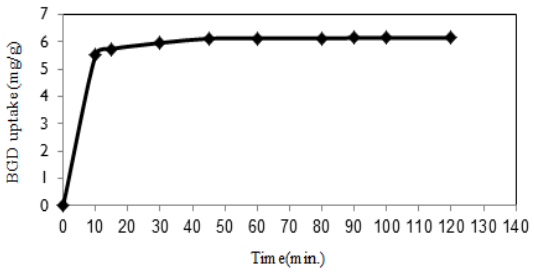

Fig. 7. Contact time effect on uptake (mg/g) of BGD using WP (dose= 0.8 g, initial BGD concentration=50 mg/l, pH 8, 250 rpm for 120 min.).

3.2.3. The influence of biosorbent dose

The uptake of BGD was discussed as a function of biosorbent dose for a given initial BGD concentration. Figure 8 illustrates the uptake and percentage removal of dye using WP. The removal efficacy of dye increased from 67.1 to 99.54%, as the biosorbent amount was increased from 0.05 to 1.4g/100 ml with keeping other factors constant. This is due to a more active site's existence for BGD removal.

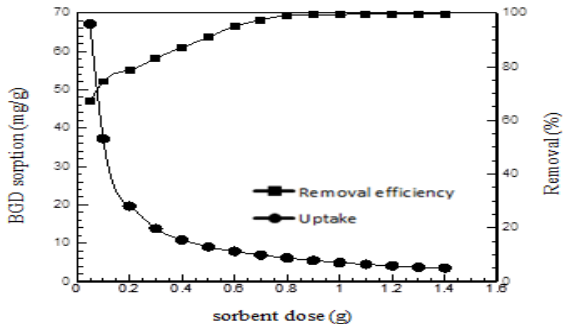

Fig. 8. Percentage removal and uptake of BGD ions in terms of biosorbent dose with initial dye concentration = 50 mg/g, pH 8, 250 rpm using WP with a contact time of 60 min.

The best dose of WP was chosen as 0.8 grams as removal efficiency increased up to 98.35%, then stayed closely constant regardless of the increase in the biosorbent amount when it did not cause a significant increase in dye removal. This can be interpreting as the greatest dye ions are sorbed onto biosorbent and the equilibrium time was reached between dye sorbed onto WP and those remaining in the solution. On the other hand, the biosorbed BGD amount per amount of biosorbent frequently decreased, because a great amount of biosorbent reduced the unsaturation of the active sites, then the total active sites per amount lowered led a lower biosorption rate to a greater amount of biosorbent. A similar fact was reported by an earlier study by Hameed. Thus, the dose of 0.8 g/100 ml was chosen for BGD removal using WP in the following experiments.

3.2.4. The influence of initial BGD concentration

The uptake, as well as percentage removal as a function of initial dye concentration with values of 10-100 mg/l for BGD biosorption, were investigated and Fig. 9 shows the results for using WP. The removal of dye lowered from 100 to 95% as the strength of dye solution increased from 10 to 100 mg/l due to the fact that at a fixed amount of biosorbent, a fixed biosorption area was existing for dye at higher initial dye concentration and a greater competitive happens by the BGD ions remaining in the liquid media to be retained by the active binding sites of the biosorbent [58]. Equilibrium between the biosorbent dose and the BGD concentration must be achieved through the best conditions for effective sorbate removal. On the other hand, the biosorption capacity increased from 1.25 to 12.22 mg g^{-1} as the initial dye concentration increased from 10 to 100 mg/l. These results can be interpreted by two main parameters, namely a great rate of BGD diffusing onto the biosorbent surface and a high possibility of collision between BGD ions and WP surface. At high initial concentration, the mass transfer resistance is reduced throughout the driving force's acceleration.

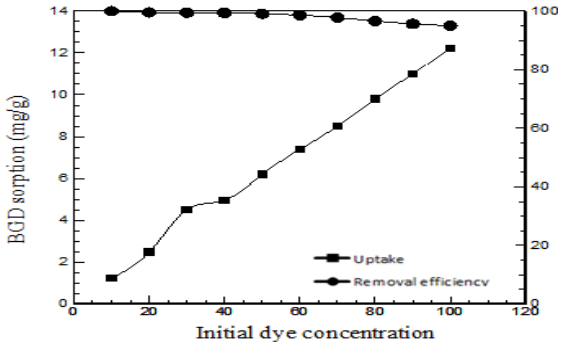

Fig. 9. Percentage removal and uptake of BGD ions as a function of BGD concentration (pH 8, 250 rpm) using WP with dose = 0.8 g/100 ml, and contact time = 60 min.

3.3. Mathematical modeling

3.3.1. Biosorption isotherm studies

It is necessary for practical tenders to forecast the complete adsorption behaviour and assess the maximum contaminant amount sequestrated from wastewater. So, the equilibrium isotherm plays a key role in the design of adsorption process when it has offered useful facts regarding adsorption under optimum conditions. Isotherm analysis displays the way of interactions between the pollutant molecules and the adsorbent. Also, it provides information about the nature of interactions in the phases of solid-liquid during the equilibrium state [61]. The experimental isotherm data of BGD biosorption onto WP were examined depending on the isotherm linear forms of Langmuir model (Eq. (3)) and Freundlich (Eq. (4)) and the obtained results are explained in Fig. 10(a) and (b), respectively. The first model assumes monolayer sorption of sorbate on the surface of sorbent with homogeneous nature, and the definite localized active sites without interaction between molecules removed on adjacent sites. It was limited sorption capacity for sorbent and no additional sorption can take place by a site and reaches an equilibrium state when the full uptake of the sorbent is attained. The Langmuir model with linear formula is described by Eq. (3):

$$\frac{C_e}{q_e} = \frac{1}{q_m K_a} + \frac{C_e}{q_m} \tag{3}$$

where the dye concentration (mg l^{-1}) at equilibrium is assigned by C_e and the adsorbate mass that adsorbed per mass of adsorbent (mg g^{-1}) is assigned by q_e while Langmuir constants (k_a (l mg^{-1}) and q_m (mg g^{-1})) which refer to the site's affinity for dye adsorption and the maximum monolayer uptake. These constants can be found by the sketch between C_e/q_e and C_e which provides a straight line with a slope ($1/q_m$) and intercept ($1/q_m k_a$) as presented in Fig. 10 and the values of constants are recorded in Table 3.

The maximum uptake, q_m, was and for BGD biosorption per gram of WP. The equilibrium data were the finest fitting with the model of Langmuir indicates of monolayer biosorption behaviour onto the biosorbent.

The dimensionless separation factor expresses the adsorption feasibility of the adsorbent, R_L, related to the Langmuir model using Eq. (4):

$$R_L = \frac{1}{1 + K_L + C_o} \tag{4}$$

As C_o is the primary BGD concentration (mg l^{-1}).

RL can indicate the isotherm shape as favourable ($0< R_L<1$), unfavourable ($R_L>1$), irreversible ($R_L=0$), and linear ($R_L=1$). The R_L values for BGD biosorption are shown in Fig. 11. The biosorption process of BGD onto WP was favourable as the R_L values were in the range of 0-1.

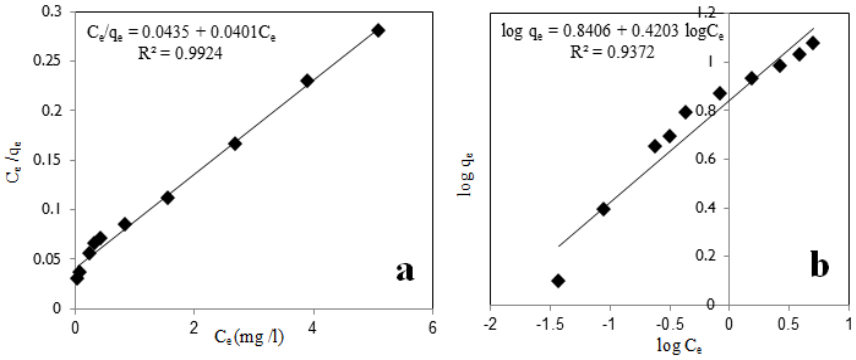

Fig. 10. Linearized model of BGD removal using WP by: (a) Langmuir isotherm (b) Freundlich isotherm.

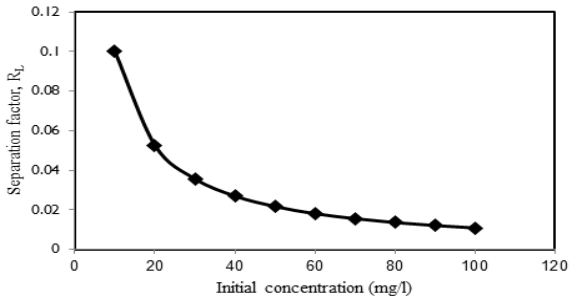

Fig. 11. RL values for BGD biosorption onto WP.

Freundlich isotherm model is an empirical form often adopted to explain that the sorption happens on heterogeneous surfaces and the energy of sorption is different. This equation describes the physisorption as the sorbed molecules interacted through the formation of multilayer sorption and are not definite to monolayer creation of sorbate molecules (chemisorption) adsorbent [61]. The Freundlich model with linear formula is described by Eq. (5):

$$\log q_e = \log K_F + \frac{1}{n} \log C_e \tag{5}$$

The model constants are K_F (mg/g)(l/mg)$^{1/n}$ and $1/n$, the first assigns to the uptake and the second indicate the surface heterogeneity [61]. Freundlich constants can be found by the intercept and slope of the sketch between ln q_e, and ln C_e as presented in Fig. 10. Constants values of this model are arranged in Table 4.

The factor (1/*n*) is a character of the heterogeneity of the sorbent surface and it converts further heterogeneous as the value of 1/n near zero. The BGD biosorption is considered to be promising as *n* inserting in the range of 1-10.

Table 4. Constants of biosorption isotherm for BGD using WP.

Langmuir		**Freundlich**	
q_m **(mg g^{-1})**	25	K_F**(mg g^{-1})(l/mg)$^{1/n}$**	6.92
K_a **(l mg^{-1})**	0.91	**1/*n***	0.42
S.E.	0.0078	***S.E.***	0.0818
R_L	0.1 - 0.0109)	**Equation**	$q_e = 6.92C_e^{0.42}$
Equation	$q_e = 22.75C_e$ / 1+0.91C_e		

The maximum biosorption capacity of WP obtained by this work was compared with other works as listed in Table 5. The value of maximum uptake (q_m) of WP is higher, so WP can be used as an efficient biosorbent to remove BGD from aqueous solutions.

Table 5. The Langmuir uptake (q_m, mg g^{-1}) comparison with the other works of utilizing agricultural wastes for BGD removal.

Adsorbent	q_m **(mg g^{-1})**	**Reference**
Rice husk ash	21.6	[62]
Acorn	2.1	[63]
Peanut shell	19.92	[62]
Strychnos potatorum	40.0	[8]
Watermelon peels (WP)	25	The present study

The experimental data and those calculated by two linear models are presented in Fig. 12. The uptake increased with a rise of equilibrium concentration with the nonlinear trend and the experimental data is more simulated by the Langmuir model with high R^2 and less value of the standard error of the estimate (S.E.). Lastly, the operation of the adsorption units faces many problems, such as the depletion of active sites, which requires continuous monitoring. For this purpose; electro-magnetic sensors could be effectively used basing on their good performance in many fields of industry, such as construction [64-66], communication [67], and water industries [68].

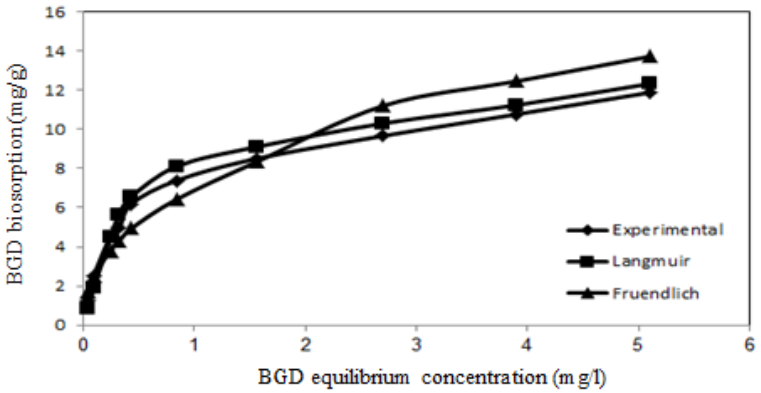

Fig. 12. Experimental and calculated biosorption capacity of BGD by Langmuir and Freundlich equilibrium isotherm models using WP.

4. Conclusions

In this work, the environmentally friendly agro-waste (WP) was utilized as biosorbent to get rid of brilliant green dye from effluents.

- Surface characterization of biosorbent before and after BGD removal was performed byways of S_{BET}, FTIR, SEM, and SPM examination.
- The operating factors, solution pH, contact time, the mass of biosorbent, and the primary strength of BGD solution were effective in removing BGD onto WP.
- The Langmuir isotherm model was better to simulate the equilibrium data and the maximum monolayer biosorption capacity of WP was 25 mg/g.
- All findings demonstrated that WP can be employed as a low-cost agro-waste to sequestrate the BGD from aqueous media.

Acknowledgements

We are grateful to Babylon University for the financial support made available for this research. The authors are also thankful to the Central Laboratory of Pharmacy College of the University of Kufa-Iraq for carrying out the necessary FTIR analysis.

Nomenclatures

q_e	Dye amount sorbed per unit amount of biosorbent, mg g^{-1}
BET	Brunauer-Emmett-Teller
C_o	Primary dye concentration, mg l^{-1}
C_e	Equilibrium dye concentration, mg l^{-1}
KF	Freundlich constant refers to uptake, (mg g^{-1})(l mg^{-1})$^{1/n}$
k_a	Langmuir constant assigns to the binding places affinity for sequestration, l mg^{-1}
1/*n*	Freundlich constant refers to surface heterogeneity
M	Biosorbent quantity, g
pH_{pzc}	Point zero charge
qm	Langmuir constant refers to monolayer full adsorption capability, mg g^{-1}
R%	Dye removal efficiency
RL	Factor of separation
R^2	Coefficient of determination
rpm	Revolution per minute
Sa	Roughness average, nm
Ssk	Surface skewness
Sar	Surface area ratio
Sk	Core roughness depth, nm
V	Dye solution volume, l

Abbreviations

AFM	Atomic force microscopy
BGD	Brilliant green dye
FTIR	Fourier transformed infrared
SBET	Specific surface area, m^2 g^{-1}
SEM	Scanning electron microscopy

SPM	Scanning probe microscope
WP	Watermelon peels

References

1. Hashim, K.S.; Hussein, A.H.; Zubaidi, S.L.; Kot, P.; Kraidi, L.; Alkhaddar, R.; Shaw, A.; and Alwash, R. (2019). Effect of initial pH value on the removal of reactive black dye from water by electrocoagulation (EC) method. *Proceedings of the* 2*nd International Scientific Conference*, Al-Qadisiyah University, Iraq 12-22.
2. Abdulhadi, B.A.; Patryk, K.; Kahlid, H.S.; Shaw, A.; and Khaddar, R.A. (2019). Influence of current density and electrodes spacing on reactive red 120 dye removal from dyed water using electrocoagulation / electroflotation (EC/EF) process. *Proceedings of the First International Conference on Civil and Environmental Engineering Technologies* (*ICCEET*), University of Kufa, Iraq, 12-22.
3. Safaa, K.S.; Al-Saati, N.H.; Alquzweeni, S.S.; Kraidi, L.; Hussein, A.H.; and Alwash, R. (2019). Decolourization of dye solutions by electrocoagulation: an investigation of the effect of operational parameters. *Proceedings of the First International Conference on Civil and Environmental Engineering Technologies* (*ICCEET*), University of Kufa, Iraq, 25-32.
4. Zubaidi, S.L.; Al-Bugharbee, H.; Muhsen, Y.R.; and Aljaaf, A.J. (2019). The Prediction of municipal water demand in Iraq: A case study of Baghdad Governorate. *Proceedings of the* 12*th International Conference on Developments in eSystems Engineering* (*DeSE*), Kazan, Russia, 274-277.
5. Zubaidi, S.L.; Abdellatif, M.; and Muhsin, Y.R. (2019). Using LARS-WG model for prediction of temperature in Columbia City, USA. *Proceedings of the IOP Conference Series: Materials Science and Engineering*, Kufa, Iraq, 1-12.
6. Salah, Z.; Abdulkareem, I.H.; Al-Bugharbee, H.; Ridha, H.M.; Gharghan, S.K.; Al-Qaim, F.F.; and Muradov, M. (2020). Hybridised artificial neural network model with slime mould algorithm: A novel methodology for prediction urban stochastic water demand. *Water*, 12(10), 1-18.
7. Hashim, K.S.; AlKhaddar, R.; Shaw, A.; Kot, P.; Al-Jumeily, D.; Alwash, R.; and Aljefery, M.H. (2020). *Advances in water resources engineering and management.* Chapter: Electrocoagulation as an eco-friendly river water treatment method. Springer, Singapore, 219-235.
8. Alenazi, M.; Hashim, K.S.; Hassan, A.A.; Muradov, M.; Kot, P.; and Abdulhadi, B. (2020). Turbidity removal using natural coagulants derived from the seeds of strychnos potatorum: statistical and experimental approach. *Proceedings of the IOP Conference Series: Materials Science and Engineering*, Kufa, Iraq, 1-14.
9. Al-Saati, N.H.; Hussein, T.K.; Abbas, M.H.; Al-Saati, Z.N.; Sadique, M.; Aljefery, M.H.; and Carnacina, I. (2019). Statistical modelling of turbidity removal applied to non-toxic natural coagulants in water treatment: a case study. *Desalination and Water Treatment*, 150, 406-412.
10. Omran, I.I.; Al-Saati, N.H.; Al-Saati, Z.N.; Ruddock, F.; and Aljefery, M. (2019). Assessment of heavy metal pollution in the Great Al-Mussaib irrigation channel. *Desalination and Water Treatment*, 168, 165-174.
11. Mohammed, A.H.; Hussein, A.H.; Yeboah, D.; Abdulhadi, B.; Shubbar, A.A.; and Khalid, K.S. (2020). Electrochemical removal of nitrate from wastewater.

Proceedings of the IOP Conference Series: Materials Science and Engineering, Kufa, Iraq, 22-32.

12. Zanki, A.K.; Mohammad, F.H.; Kareem, M.M.; and Abdulhadi, B. (2020). Removal of organic matter from water using ultrasonic-assisted electrocoagulation method. *Proceedings of the IOP Conference Series: Materials Science and Engineering*, Thi-Qar, Iraq, 22-32.
13. Aqeel, K.; Mubarak, H.A.; Amoako-Attah, J.; Abdul-Rahaim, L.A.; Abdellatif, M.; and Al-Janabi, A. (2020). Electrochemical removal of brilliant green dye from wastewater. *Proceedings of the IOP Conference Series: Materials Science and Engineering*, Instanbul, Turky, 15-23.
14. Emamjomeh, M.M.; Mousazadeh, M.; Mokhtari, N.; Jamali, H.A.; Makkiabadi, M.; Naghdali, Z.; and Ghanbari, R. (2020). Simultaneous removal of phenol and linear alkylbenzene sulfonate from automotive service station wastewater: Optimization of coupled electrochemical and physical processes. *Separation Science and Technology*, 55(17), 3184-3194.
15. Alenezi, A.K.; Hasan, H.A.; Amoako-Attah, J.; Gkantou, M.; Muradov, M.; and Bareq, B. (2020). Zeolite-assisted electrocoagulation for remediation of phosphate from calcium-phosphate solution. *Proceedings of the IOP Conference Series: Materials Science and Engineering*, Babylon, Iraq, 13-15.
16. Alyafei, A.; AlKizwini, R.S.; Yeboah, D.; Gkantou, M.; Al-Faluji, D.; and Salah, S.L. (2020). Treatment of effluents of construction industry using a combined filtration-electrocoagulation method. *Proceedings of the IOP Conference Series: Materials Science and Engineering*, Tikrit, Iraq, 63-77.
17. Abdulhadi, B.; Muradov, M.; and Al-Khaddar, R. (2021). Continuous-flow electrocoagulation (EC) process for iron removal from water: Experimental, statistical and economic study. *Science of the Total Environment*, 756(2), 1-16.
18. Hashim, K.S.; Andrew, S.; Mustafa, R.; and Al-Shamma'a, A. (2021). Water purification from metal ions in the presence of organic matter using electromagnetic radiation-assisted treatment. *Journal of Cleaner Production*, 280(2), 1-17.
19. Al-Marri, S.; AlQuzweeni, S.S.; AlKizwini, R.S.; Zubaidi, S.L.; and Al-Khafaji, Z.S. (2020). Ultrasonic-Electrocoagulation method for nitrate removal from water. *Proceedings of the IOP Conference Series: Materials Science and Engineering*, Istanbul, Turkey, 101-114.
20. Safaa, K.H.; Ali, S.M.; AlRifaie, J.K.; Idowu, I.; and Gkantou, M. (2020). Escherichia coli inactivation using a hybrid ultrasonic-electrocoagulation reactor. *Chemosphere*, 247, 125868-125875.
21. Hassan Alnaimi, J.I.; Abuduljaleel, J.; Khalid, S.K.; Michaela, G.; Magomed, M. (2020). Ultrasonic-electrochemical treatment for effluents of concrete plants Ultrasonic-electrochemical treatment for effluents of concrete plants. *Proceedings of the IOP Conference Series Materials Science and Engineering*, University of Kufa, Najaf, Iraq, 1-9.
22. Alhendal, M.; Nasir, M.J.; Amoako-Attah, J.; Al-Faluji, D.; Muradov, M.; and Abdulhadi, B. (2020). Cost-effective hybrid filter for remediation of water from fluoride. *Proceedings of the IOP Conference Series: Materials Science and Engineering*, Babylon, Iraq, 77-88.
23. Ortoneda, P.M.; and Phipps, D. (2017). Defluoridation of drinking water using a new flow column-electrocoagulation reactor (FCER) - Experimental,

statistical, and economic approach. *Journal of Environmental Management*, 197, 80-88.

24. Hussein, A. H.; and Al-Saati, Z. N. (2018). An investigation into the level of heavy metals leaching from canal-dreged sediment: A case study metals leaching from dreged sediment. *Proceedings of the First International Conference on Materials Engineering & Science*, Istanbul Aydın University (IAU), Turkey, 12-22.
25. Idowu, I. A.; Jasim, N.; Phipps, D.; Kot, P.; Pedrola, M. O.; Alattabi, A. W.; and Abdulredha, M. (2018). Removal of phosphate from river water using a new baffle plates electrochemical reactor. *MethodsX*, 5, 1413-1418.
26. Shaw, A.; Pedrola, M. O.; and Phipps, D. (2017). Iron removal, energy consumption and operating cost of electrocoagulation of drinking water using a new flow column reactor. *Journal of Environmental Management*, 189, 98-108.
27. Pedrola, M.O.; and Phipps, D. (2017). Energy efficient electrocoagulation using a new flow column reactor to remove nitrate from drinking water - Experimental, statistical, and economic approach. *Journal of Environmental Management*, 196, 224-233.
28. Alattabi, A.W.; Harris, C.; and Alzeyadi, A. (2017). Treatment of residential complexes' wastewater using environmentally friendly technology. *Procedia Engineering*, 196, 792-799.
29. Alattabi, A.W.; Harris, C.B.; Ortoneda-Pedrola, M.; and Phipps, D. (2017). Improving sludge settleability by introducing an innovative, two-stage settling sequencing batch reactor. *Journal of Water Process Engineering*, 20, 207-216.
30. Abdulla, G.; Kareem, M.M.; Hashim, K.S.; Muradov, M.; Kot, P.; Mubarak, H.A.; Abdellatif, M.; and Abdulhadi, B. (2020). Removal of iron from wastewater using a hybrid filter. *Proceedings of the IOP Conference Series: Materials Science and Engineering*, 012035.
31. Abdulraheem, F.S.; Al-Khafaji, Z.S.; Hashim, K.S.; Muradov, M.; Kot, P.; and Shubbar, A. A. (2020). Natural filtration unit for removal of heavy metals from water. *Proceedings of the IOP Conference Series: Materials Science and Engineering*, 012034.
32. Abdulhadi, B. (2020). Continuous-flow electrocoagulation (EC) process for iron removal from water: Experimental, statistical and economic study. *Science of The Total Environment*, 143417.
33. Emamjomeh, M.M.; Kakavand, S.; Jamali, H.A.; Alizadeh, S.M.; Safdari, M.; Mousavi, S.S.; and Mousazade, M. (2020). The treatment of printing and packaging wastewater by electrocoagulation-flotation: the simultaneous efficacy of critical parameters and economics. *Desalination and water treatment*, 205, 161-174.
34. Al-Jumeily, D.; and Aljefery, M. (2020). Energy efficient electrocoagulation using baffle-plates electrodes for efficient *Escherichia Coli* removal from wastewater. *Journal of Water Process Engineering*, 33(20), 101079-101086.
35. Salleh, A.M.; Mahmoud, D.K.; Karim, W.A.; and Idris, A. (2011). Cationic and anionic dye adsorption by agricultural solid wastes: A comprehensive review. *Desalination*, 280(1-3), 1-13.
36. Ewadh, H.M.; Muhsin, A.A.; and Aljefery, M. (2020). Phosphate removal from water using bottom ash: Adsorption performance, coexisting anions and modelling studies. *Water Science and Technology*, 82(11), 1-17.

37. Jasim, N.; Shaw, A.; Phipps, D.; Alattabi, A.W.; and Alawsh, R. (2019). Electrocoagulation as a green technology for phosphate removal from River water. *Separation and Purification Technology*, 210, 135-144.
38. Weng, C.H.; Lin, Y.T.; and Tzeng, T.W. (2009). Removal of methylene blue from aqueous solution by adsorption onto pineapple leaf powder. *Journal of hazardous materials*, 170(1), 417-424.
39. Jawad, A.H.; Ngoh, Y.; and Radzun, K.A. (2018). Utilization of watermelon (Citrullus lanatus) rinds as a natural low-cost biosorbent for adsorption of methylene blue: kinetic, equilibrium and thermodynamic studies. *Journal of Taibah University for Science*, 12(4), 371-381.
40. Al-Bugharbee, H.; Gharghan, S.; Olier, I.; and Al-Bdairi, N. (2020). A novel methodology for prediction urban water demand by wavelet denoising and adaptive neuro-fuzzy inference system Approach. *Water*, 12(6), 1-17.
41. Ethaib, S.; Al-Bdairi, N.S.; and Gharghan, S.K. (2020). A novel methodology to predict monthly municipal water demand based on weather variables scenario. *Journal of King Saud University-Engineering Sciences*, 32(7), 1-18.
42. Ortega-Martorell, S.; Abdellatif, M.; Gharghan, S.K.; and Ahmed, M.S. (2020). A method for predicting long-term municipal water demands under climate change. *Water Resources Management*, 34(3), 1265-1279.
43. Grmasha, R.A.; Al-sareji, O.J.; Salman, J.M.; and Jasim, I.A. (2020). Polycyclic aromatic hydrocarbons (PAHs) in urban street dust within three land-uses of Babylon Governorate, Iraq: Distribution, sources, and health risk assessment. *Journal of King Saud University - Engineering Sciences*, 33, 1-18.
44. Muhsin, Y.R. (2020). Forecasting of monthly stochastic signal of urban water demand: Baghdad as a case study. *Proceedings of the IOP Conference Series: Materials Science and Engineering*, Istanbul, Turkey, 89-97.
45. Ortega-Martorell, S.; Olier, I.; and Gharghan, S.K. (2020). Urban water demand prediction for a city that suffers from climate change and population growth: Gauteng Province case study. *Water*, 12(7), 1-18.
46. Kadhim, A.; Sadique, M.; and Al-Mufti, R. (2020). Developing one-part alkali-activated metakaolin/natural pozzolan binders using lime waste as activation agent. *Advances in Cement Research*, 32(11), 1-38.
47. Majdi, H.S.; Shubbar, A.; Nasr, M.S.; Al-Khafaji, Z.S.; Jafer, H.; Abdulredha, M.; Masoodi, Z.A.; and Sadique, M. (2020). Experimental data on compressive strength and ultrasonic pulse velocity properties of sustainable mortar made with high content of GGBFS and CKD combinations. *Data in Brief*, 31, 105961-105972.
48. Shubbar, A.A.; Sadique, M.; Nasr, M.S.; and Al-Khafaji, Z.S. (2020). The impact of grinding time on properties of cement mortar incorporated high volume waste paper sludge ash. *Karbala International Journal of Modern Science*, 6(4), 1-23.
49. Shubbar, A.A.; Jafer, H.; Dulaimi, A.; Atherton, W.; and Sadique, M. (2018). The development of a low carbon binder produced from the ternary blending of cement, ground granulated blast furnace slag and high calcium fly ash: An experimental and statistical approach. *Construction and Building Materials*, 187, 1051-1060.
50. Shubbar, A.A.; Al-Shaer, A.; AlKizwini, R.S.; Hawesah, H.A.; and Sadique, M. (2019). Investigating the influence of cement replacement by high volume

of GGBS and PFA on the mechanical performance of cement mortar. *Proceedings of the First International Conference on Civil and Environmental Engineering Technologies* (*ICCEET*), University of Kufa, Iraq, 31-38.

51. Kadhim, A.; Sadique, M.; Al-Mufti, R ; and Hashim, K.. (2020). Long-term performance of novel high-calcium one-part alkali-activated cement developed from thermally activated lime kiln dust. *Journal of Building Engineering*, 32, 101766.
52. Shubbar, A.A.; Sadique, M.; Shanbara, H.K.; and Hashim, K. (2020). *Advances in Sustainable Construction materials and geotechnical engineering*. Chapter: The development of a new low carbon binder for construction as an alternative to cement. Springer, Singapore.
53. Al-Jumeily, D.; Hashim, K.; Alkaddar, R.; Al-Tufaily, M.; and Lunn, J. (2018). Sustainable and environmental friendly ancient reed houses (Inspired by the past to motivate the future). 2018 11*th International Conference on Developments in eSystems Engineering* (*DeSE*), Cambridge, UK, 214-219.
54. Abdulredha, M.; Alkhaddar, R.A.L.; Jordan, D.; and Hashim, K. (2017). The development of a waste management system in Kerbala during major pilgrimage events: determination of solid waste composition. *Procedia Engineering*, 196, 779-784.
55. Abdulredha, M.; Alkhaddar, R; Jordan, D.; Kot, P.; Abdulridha, A.; and Hashim, K. (2018). Estimating solid waste generation by hospitality industry during major festivals: A quantification model based on multiple regression. *Waste Management*, 77, 388-400.
56. Idowu, I.A.; Atherton, W.; Hashim, K.; Kot, P.; Alkhaddar, R; Alo, B.I.; and Shaw, A. (2019). An analysis of the status of landfill classification systems in developing countries: Sub Saharan Africa landfill experiences. *Waste Management*, 87, 761-771.
57. Lakshmipathy, R.; and Sarada, N. (2016). Methylene blue adsorption onto native watermelon rind: batch and fixed bed column studies. *Desalination and Water Treatment*, 57(23), 10632-10645.
58. Mudzielwana, R.; Gitari, W.; and Msagati, T. (2016). Intercalation of Mn 2+ ions onto bentonite clay: Implications in groundwater defluoridation. *WIT Transactions on Ecology and the Environment*, 209, 151-160.
59. Brunauer, S.; Emmett, P.H.; and Teller, E. (1938). Adsorption of gases in multimolecular layers. *Journal of the American chemical society*, 60(2), 309-319.
60. Mohammed, A.A.; and Samaka, I.S. (2018). Bentonite coated with magnetite Fe3O4 nanoparticles as a novel adsorbent for copper (II) ions removal from water/wastewater. *Environmental Technology & Innovation*, 10, 162-174.
61. Mohammed, A.A.; Brouers, F.; Samaka, I.S.; and Al-Musawi, T.J. (2018). Role of Fe_3O_4 magnetite nanoparticles used to coat bentonite in zinc (II) ions sequestration. *Environmental Nanotechnology, Monitoring & Management*, 10, 17-27.
62. Aadil, A.; Shahzad, M.; Kashif, S.; Muhammad, M.; Rabia, A.; and Saba, A. (2012). Comparative study of adsorptive removal of congo red and brilliant green dyes from water using peanut shell. *Middle East Journal of Scientific Research*, 11(6), 828-832.
63. Ghaedi, M.; Hossainian, H.; Montazerozohori, M.; Shokrollahi, A.; Shojaipour, F.; Soylak, M.; and Purkait, M. (2011). A novel acorn based adsorbent for the removal of brilliant green. *Desalination*, 281, 226-233.

64. Gkantou, M.; Muradov, M.; Kamaris, G.S.; and Atherton, W. (2019). Novel electromagnetic sensors embedded in reinforced concrete beams for crack detection. *Sensors*, 19(23), 5175-5189.
65. Teng, K.H.; and Al-Shamma'a, A. (2019). Embedded smart antenna for non-destructive testing and evaluation (NDT&E) of moisture content and deterioration in concrete. *Sensors*, 19(3), 547-559.
66. Omer, G.; Kot, P.; Atherton, W.; Muradov, M.; Gkantou, M.; Shaw, A.; Riley, M.; Hashim, K.; and Al-Shamma'a, A. (2020). A non-destructive electromagnetic sensing technique to determine chloride level in maritime concrete. *Karbala International Journal of Modern Science*, 7(1), Article 8.
67. Ryecroft, S.P.; Fergus, P.; Moody, A.; and Conway, L. (2019). A first implementation of underwater communications in raw water using the 433 MHz frequency combined with a bowtie antenna. *Sensors*, 19(8), 1813-1823.
68. Ryecroft, S.P.; Fergus, P.; and Conway, L. (2019). A novel gesomin detection method based on microwave spectroscopy. *Proceedings of the* 12*th International Conference on Developments in eSystems Engineering* (*DeSE*), Kazan, Russia, 429-433.